Available online at www.sciencedirect.com
ScienceDirect
ELSEVIER
Palaeogeography, Palaeoclimatology, Palaeoecology 239 (2006) 45–62
PALAEO
www.elsevier.com/locate/palaeo

A multi-proxy study of Argentina loess: Marine oxygen isotope stage 4 and 5 environmental record from pedogenic hematite

Brian Carter-Stiglitz [a,*], Subir K. Banerjee [a], Alexandra Gourlan [b], Eric Oches [c]

[a] *Institute for Rock Magnetism, Newton Horace Winchell School of Earth Sciences, University of Minnesota, Minneapolis, 55455, USA*
[b] *Laboratoire de Géochimie et Cosmochimie, Institut de Physique du Globe de Paris, 75252 Paris cedex 05, France*
[c] *Department of Geology, University of South Florida, Tampa 33620, USA*

Received 15 July 2005; received in revised form 1 December 2005; accepted 7 January 2006

Abstract

A 12 m loess–paleosol section (La Angostura) from Tafi del Valle, Tucumán, Argentina was studied using rock magnetic measurements, geochemistry, Mössbauer effect, particle size and Nd isotopes in order to elucidate changes in paleoenvironment at the site. Combining the results of these experiments allowed us to separate the effects of the two major controls (parent material and pedogenesis) on the measured parameters. Two behavior regimes were identified in the sediment: 1) in the lower half of the section pedogenic processes, though weak, dominate the variation of the sediment's physical properties, and 2) for the upper half of the section subtle changes in parent material control the majority of the measured parameters, even those typically controlled by pedogenesis, e.g., clay fraction. Applying rock magnetic, Mössbauer, and bulk geochemistry measurements in concert we calculated an iron budget for the loess. ~80% of the iron in the sediment is in paramagnetic minerals; ~20% of the iron is in hematite (~1.6% of the sediment's mass), and ≪1% of the total iron is present as magnetite/maghemite (~0.1% of the sediment's total mass). Neither the pedogenic formation nor the depletion of ferrimagnetic material with increasing pedogenesis was consistently observed in this sediment. Throughout the entire section the concentration of hematite is argued to be sensitive to in situ alteration, and it is further surmised to be sensitive to the available moisture at the site. Finally we present a curiosity: within the error of our chronology, the concentration of hematite seems to correlate with the coeval climate record from Antarctica (Vostok). It is possible that the sedimentary–magnetic record from La Angostura is a proxy for the strength of the South American summer monsoon.

Keywords: Environmental magnetism; Rock magnetism; Hematite; Nd isotopes; Argentina; Loess

1. Introduction

Loess deposits–which cover ~10% of the earth's surface–have provided some of the longest and most complete records of continental climate to date (Heller and Evans, 1995). The Chinese loess is, by far, the most celebrated and well studied example. Heller and Liu (1982) provided the first convincing paleomagnetic stratigraphy for the Chinese loess, establishing its potential as an archive of 2.6 million years of climatic change. Although questions still remain concerning some details of the stratigraphy (see Evans and Heller (2003)), their original chronologic framework stands,

* Corresponding author. Tel.: +1 612 625 9985.
E-mail address: cart0196@umn.edu (B. Carter-Stiglitz).

0031-0182/$ - see front matter © 2006 Elsevier B.V. All rights reserved.
doi:10.1016/j.palaeo.2006.01.008

and has been (for the youngest sediment) cross validated with luminescence age estimates (Lu et al., 1987; Forman, 1991). With an established chronology, it became clear that the variations in magnetic susceptibility (high values being associated with paleosols) strongly correlated with oxygen isotope data from ocean sediments (Heller and Liu, 1984; Liu et al., 1985; Kukla et al., 1988; Kukla and An, 1989). Initially the correlation was explained by higher concentrations of detrital ferrimagnetic material in paleosols (Heller and Liu, 1986; Kukla and An, 1989). Soon after the suggestion of these initial models it became clear that the magnetic enhancement was due to the pedogenic formation of ferrimagnetic material, especially ultra-fine (<30 nm) particles (Zhou et al., 1990; Maher and Thompson, 1991; Banerjee et al., 1993; Verosub et al., 1993; Hunt et al., 1995a). The pedogenic model is currently well accepted. Although the process which leads to the formation of this pedogenic magnetite/maghemite is not completely understood, the process is probably mediated by iron reducing bacteria (Dearing et al., 2001).

It is important to realize that the success of magnetic studies on the Chinese loess has largely been built on the characterization of the easily measured ferrimagnetic minerals (magnetite and maghemite), while other iron oxides have largely been ignored. Indeed, a consensus concerning the complete iron-mineralogy budget of the Chinese loess has not emerged. Consider hematite, the most abundant iron oxide in the Chinese loess (Eyre and Dickson, 1995; Fine et al., 1995; Hunt et al., 1995a). Based on rock magnetic measurements it was concluded that hematite is present in equal amounts in paleosol and loess (Evans and Heller, 2001; Evans and Rokosh, 2000) or even in lower amounts in paleosols (Maher and Thompson, 1991). Contrarily, an enhancement of hematite in paleosols has been observed (Eyre and Dickson, 1995; Fine et al., 1995; Hunt et al., 1995b; Ji et al., 2001). Fine et al. (1995) used a combination of rock magnetic measurements and citrate–bicarbonate–dithionite chemical treatments to calculate a complete iron budget for the Chinese loess, and suggested that hematite is nearly twice as important in paleosols as it is in loess. Ji et al. (2001) noticed that hematite concentration (as quantified by spectrophotometry) roughly correlated with magnetic susceptibility, but tended to rise before and fall after the susceptibility had changed. They suggested that the pedogenic formation of hematite and maghemite/magnetite differ—maghemite/magnetite being favored by alternating periods of sustained wetness and dryness, whereas hematite is favored in a weak monsoonal climate (precipitation > ~300 mm/yr) when short periods of wetness alternate with long warm/dry periods (Schwertmann, 1988; Maher, 1998).

In contrast to the Chinese loess, studies of Alaskan and Siberian loess have found that paleosols correspond to low values of magnetic susceptibility, i.e. the paleosols seem to be magnetically depleted (Begét et al., 1990; Chlachula et al., 1998; Vlag et al., 1999; Begét, 2001; Matasova et al., 2001). The cause of this relationship is not clear (Begét et al., 1990; Liu et al., 1999).

The most basic questions, at least in terms of environmental magnetism, that have been convincingly addressed for the Chinese loess (and to a lesser degree the Alaskan loess)–e.g., "Is the correlation between the magnetism of the loess and other climate proxies meaningful", and "Is the magnetic material enhanced in paleosols allochthonous or autochthonous"–are just beginning to be posed and addressed for the Argentine loess. Indeed, it is not even clear if there is a consistent relation between the ferrimagnetic minerals and paleosol stratigraphy in the Argentine loess.

Much of Argentina is blanketed in loess and loessoid sediments. Fig. 1 shows the distribution of loess and loessoid sediment as mapped by Terrugi (1957). Some modifications to this distribution have been suggested; the most drastic being the suggestion that a significant portion of the loess/loessoid material reported by Terrugi (1957) is actually aeolian sand (Iriondo, 1990, 1997, 1999), and also a much more limited distribution for loess from the last glaciation. In fact, Iriondo (2002) states that the Terrugi (1957) "…did not pretend to publish a detailed map, but only a sketchy illustration". Sayago et al. (2001) suggested a distribution that is a slightly modified version of that proposed by Terrugi (1957). The reader is directed to Zárate (2003) for a complete review of this problem.

Since the distribution of the Argentina loess remains debated, it is hardly surprising that the literature provides multiple viewpoints as to the source area(s) for the loess. Based on a characterization of the mineral assemblages in the loess, Terrugi (1957) suggested that the source area is dominated by pyroclastics and basalts; the most obvious candidates being the Andes Cordillera and/or Pantagonia. For the southernmost Pampa loess, Iriondo (1990) suggested that the ultimate source is the glaciated valleys of the Andes Cordillera but that the material undergoes an initial stage of fluvial transport from north to south by the Salado–Desaguadero–Curacó fluvial system which extends from 28° to 38° S. After the fluvial transport Iriondo (1990) argues that the loess is deflated and transported by southerly/SSW

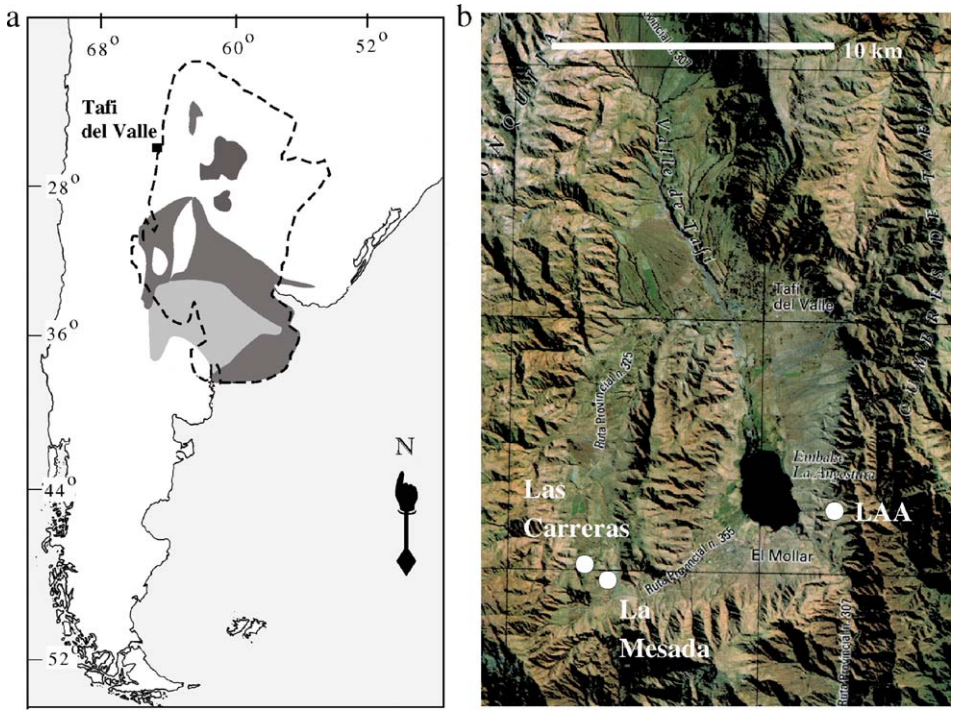

Fig. 1. a) Map showing approximate distribution of loess in Argentina. The dashed line indicates the distribution of loess and loessoid deposits as mapped by Terrugi (1957). The dark gray and light gray areas are loess and aeolian sands, respectively, as mapped by Krohling (1999), b) Tafi del Valle with the locations of LAA, La Mesada, and Las Carreras indicated.

winds. A more complicated model has emerged for the loess further north. Various studies have suggested that the northern Pampa and Chaco sediment have been derived from three separate provenances: Andes Cordillera, Sierras Pampeanas and the Paraná River basin (Krohling, 1999; Morrás, 1999; Blasi et al., 2001). Sayago (1995) advocated a single Andean/Patagonian source to the south of the Pampean loess, and transport by the southerlies.

Recent Sr and Nd isotope data seem to have limited the spectrum of possible models. Smith et al. (2003) ruled out a single Andean/Patagonian and instead suggest multiple source areas. Moreover, referring to a correlation between the latitudinal variation of ε_{Nd} in loess and Andean volcanic rocks, Smith et al. (2003) proposed direct west to east transport, be it aeolian, or a combination of fluvial and aeolian transport. The modern prevailing winds, for 27° to 37° S, are not westerly, and thus a change in prevailing wind direction is necessary to explain the eastward transport of the loess. To explain this, Smith et al. (2003) appeal to a northward movement in the Polar Front, leading to an increase in intensity and frequency of westerly winds further to the north. (Westerly winds are present in the modern weather patterns of Patagonia.) The northernmost site of their study (28.70° S), however, seems to have its source area to the northwest rather than directly to the west. Smith et al. (2003) suggest that the modern north-westerly winds which blow down slope from the Altiplano would have been augmented during glacial stages by katabatic winds generated by mountain glaciers. In combination with the subtropical jetstream, these winds were thus surmised to transport the loess from its provenance of Paleozoic gneisses and granitoids onto the Chaco Plains.

Despite its large areal extent, most of the Argentine loess sections described to date are thin and likely contain numerous unconformities (Orgeira et al., 1998; Krohling, 1999; Tonni et al., 1999; Zárate et al., 2002). Moreover, our recent field observations of loess near Buenos Aires suggest that a single welded paleosol complex can encompass several separate periods of intense pedogenesis; a similar multistage pedogenic model was suggested by Zárate et al. (2002) for a 10 m section near Buenos Aires.

An altogether different situation arises for the loess found in Tafi del Valle (1800 m asl). Tafi del Valle is a small inter-montane valley in the easternmost pre-Andes ranges; just 20 km to the east is the Gran Chaco Plain at 200 m asl. The isotope studies mentioned above suggest

a source area to the north-west, the Chilean Andes, for a site to the south east of Tafi del Valle. If correct, the source rocks for the loess in Tafi del Valle are almost certainly the same. Although the ultimate source material may lie deep in the Chilean Andes, the possibility of a very local source for the silt itself should be considered. For example, sedimentation sans loess in the valley directly to the north is dominated by a high energy braided river draining the high Andes, and could be an important source of silt.

Undisturbed loess in the valley is limited, generally restricted to mesa-like erosional relics on the valley floor. Such was the setting for the section studied by Sayago et al. (2001), La Mesada–radiocarbon dating of alkali–extract of organic material suggested that 37 m of sediment was deposited in just 10 ky. Moreover some 20 paleosols were identified, suggesting not only an abruptly changing climate, but also an amazingly quick pedogenic response. The section has since been redated by optically stimulated luminescence (OSL). The new results suggest ages much older than those in Sayago et al. (2001), and much lower sedimentation rates (Kemp et al., 2003, 2004). Kemp et al. (2003) also studied the micromorphologic features of a sequence of two paleosols from La Mesada, obtaining details concerning the stages of pedogenesis. The use of micromorphological techniques allowed the deconvolution of the complex pedogenic history of the lowest portion of the La Mesada section. The OSL age estimates (measured on fine-grained quartz) (≥ ~150 kya) of Kemp et al. (2003) are, however, near or past the maximum age limit of the technique and should probably be taken as minimum age estimates. A more exact chronology is provided by the paleomagnetic stratigraphy established for the Las Carreras section (Schellenberger et al., 2003). Schellenberger et al. (2003) were able to identify the Matuyama–Brunhes boundary as well as the Jaramillo sub-chron in the 50 m section, establishing 1.2 Ma as the minimum age for the onset of loess deposition in Tafi del Valle. Schellenberger et al. (2003) also suggested that the paleosols in the section were associated with relative lows in magnetic susceptibility, but this is not consistent throughout the entire section.

2. Site description

Besides the mesa-like loess hills on the valley floor described above, primary and reworked loess often mantle the valley walls. Our site, La Angostura (LAA), abuts the eastern valley wall in the southern portion of Tafi del Valle, on a small topographic saddle (26°56′ 40.1″ S, 65°40′3″ W, 1900 m asl) (Fig. 1). The proximity to the valley wall and the dip towards the valley center make fluvial and colluvial reworking important considerations. The location of a topographic saddle was chosen to minimize colluvial and/or fluvial resedimentation. Nevertheless two short intervals within the section, identified by the presence of matrix-supported loess-aggregate clasts, have clearly undergone resedimentation. Other than these two intervals the sediment is fairly homogenous with no clear indications of unconformities.

Modern regional precipitation is driven by the South American summer monsoon (SASM). A combination of sensible and direct heating of the central Andes, and latent heating from precipitation over the central Andes and Amazon basin, creates the Bolivian high and strong westerlies in the upper troposphere. Accompanying this is moisture-laden low-level easterly flow over the Amazon basin (Fig. 2). This flow pattern develops during the austral summer, with major precipitation between December and March (Zhou and Lau, 1998). At LAA local orography is the major control on precipitation, most of which falls on the easternmost slopes of the pre-Andean range flanking Tafi del Valle 5 km to the east. These slopes, with precipitation ~2000 mm/yr, are mantled with tropical forests, while

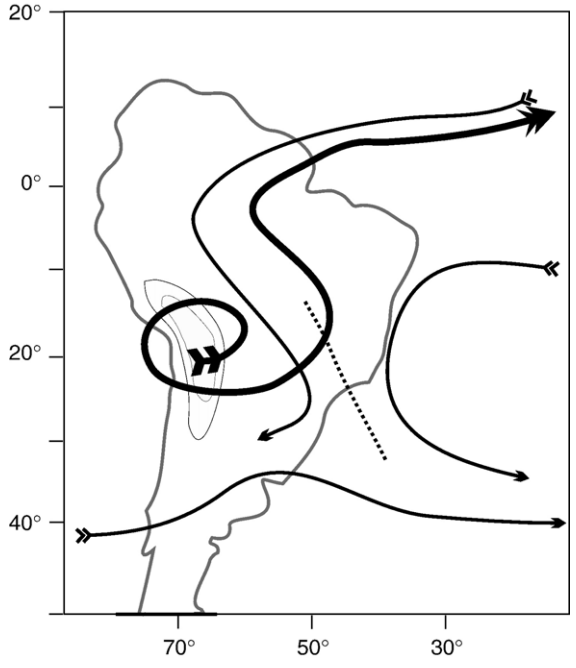

Fig. 2. Schematic of the South American summer monsoon (Zhou and Lau, 1998). The heavy lined arrow indicates upper troposphere flow (200 hPa), and the thin lined arrows indicate low troposphere flow (840 hPa). The dashed line indicates the South Atlantic convergence zone.

grasslands cover the Gran Chaco plain below, and sparse xerophytic vegetation occupies the intra-Andean regions like Tafi del Valle, with precipitation ~200 mm/yr (Trauth et al., 2000).

3. Stratigraphy

The sampled part of the LAA section is 10 m thick and contains numerous paleosol complexes (Fig. 3). The uppermost two meters of the profile are resedimented soil and were not sampled. Both paleosols and loess horizons exhibit a weak degree of alteration. Therefore drawing a clear distinction between the two in the field can be problematic. Nevertheless paleosols were identified in the field based on color and weak soil structure, largely granular to small sub-angular blocky structure. The lower and upper limits for the paleosols at 6.5 m and 4 m, respectively, were especially difficult to identify. The paleosol at 4 m is most likely an accretionary soil formed as loess deposition increased in intensity.

3.1. Chronology

The chronology for the LAA section is provided by four OSL age estimates obtained from separated silt-sized quartz grains. (Dating was done by E. Rhodes, Luminescence Dating Laboratory, Research Laboratory for Archaeology and the History of Art, University of Oxford.) The samples were taken from layers identified as relatively unaltered (Fig. 3). Silt-sized quartz was isolated from the bulk by a prolonged bath in 35% H_2SiF_6. It is worth noting that after the laboratory's standard two week treatment the samples still produced a significant infra-red stimulated luminescence (IRSL), indicating the persistent presence of feldspars. After a second treatment, the samples displayed low IRSL signals and reproducible results. The single-aliquot regeneration method (Murray and Wintle, 2000) was used in all cases and OSL measurements were made at 125 °C for 100 s using automated Risø luminescence equipment. Irradiation was accomplished using a sealed ^{90}Sr source at rates of 1.5–3 Gy/min. Concentrations of U, Th, and K were quantified using neutron activation analysis. Dose rates were then calculated using the

Table 1

OSL sample depth (m)	Total dose rate (Gy/ka)	D_e (Gy)	Age (kya)
3.40	5.032±0.26	324±18	64±5
5.80	5.193±0.28	370±22	71±5
7.50	4.792±0.26	395±5	82±5
10.40	4.587±0.24	428±12	93±6

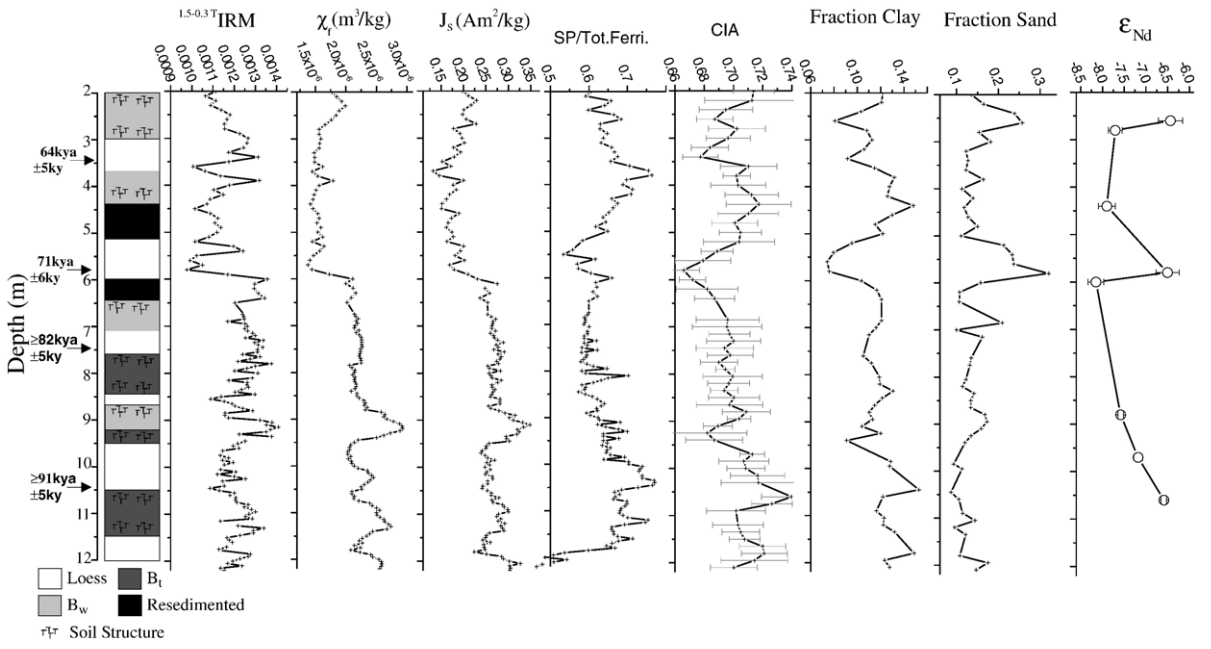

Fig. 3. Stratigraphy, OSL age estimates, rock magnetic measurements, weathering index, particle size data, and Nd isotopes for the loess section at LAA. χ_f, the ferrimagnetic susceptibility, is the total susceptibility less the high-field susceptibility determined from hysteresis loops. The chemical index of alteration (CIA) is defined as: $Al_2O/[Al_2O+CaO+Na_2O+K_2O]$. Paleosols which grade into loess or loess which grades into paleosols are indicated with a gradient in the paleosol grayscale.

standard conversion factors (Adamiec and Aitken, 1998). Table 1 summarizes the results of the OSL dating. (D_e is the equivalent dose.) The two oldest dates are near the limit of the OSL technique and should be considered minimum age estimates.

4. Experimental methods and results

Numerous magnetic and non-magnetic techniques were employed to characterize the loess–paleosol section at LAA. The mineralogy, concentration, grain size, and origin of the iron-bearing minerals in the loess are the central foci of the analytical results shown. Mössbauer spectra (obtained with a ^{57}Co calibrated with iron foil) were measured for bulk samples at 300 and at 77 K, and for magnetic extracts at 300 K. X-ray diffraction (Cu radiation) was measured for bulk samples and for magnetic extracts. Major element geochemistry was measured for bulk samples with an inductively coupled plasma mass spectrometer. Thin sections (approximately 30 μm thick) were made by impregnating unoriented peds with epoxy. Elemental maps (measured on thin sections) were made with a JEOL microprobe. Particle size was measured using a "LA-920" laser diffractometer system manufactured by Horiba Instruments, Inc. An optical model appropriate for quartz was used, as quartz was the major mineral component identified in the X-ray diffraction patterns. Samples were dispersed by gently crushing in a mortar and pestle, and shaking overnight in a solution of 5×10^{-3} kg/L sodium hexametaphosphate (HMP); the samples were measured in a solution of 0.5×10^{-3} HMP, and ultrasonically dispersed for 40 s using the instrument's inline sonicator prior to measurement. Chemical pretreatments to remove organic carbon and carbonates were not used because total carbon was less than 0.5%. Citrate bicarbonate dithionite (CBD) was used to remove iron for a handful of pilot samples, but the end results were identical to those obtained using only HMP and thus the CBD pretreatment was abandoned. Particle size data were analyzed using the GRADISTAT program (Blott and Pye, 2001).

Nd isotopic analyses were performed on ~60 mg subsamples of the loess. The biogenic carbonate fraction, owing to its small proportion, has no influence in the Nd isotopic composition. Thus the biogenic carbonate was dissolved with HCl at room temperature in order to avoid CaF_2 precipitates in the following steps. The residue was dried and organic matter was removed by oxidation through drop-wise addition of H_2O_2 at 90 °C. Samples were dissolved using screw-top Savillex Teflon beakers and a HNO_3–HF–$HClO_4$ mixture at 145 °C for 2–3 days. Concentrations were determined for all samples by isotope dilution using ^{149}Sm–^{150}Nd spikes. The rare earth elements (REEs) were separated as a group on a transuranic specific resin (Eichrom® Truspec) using a HNO_3 2 N solution. Then, the residue was dissolved in 0.225 N HCl for subsequent column chemical separation on a REE specific resin (Eichrom® Ln-Spec). Isotopic ratios were measured on a multi-collector ICP-MS (Neptune) at the Institut de Physique du Globe de Paris. Nd isotopic ratios were corrected for instrumental fractionation according to an exponential law relative to ^{146}Nd/^{144}Nd=0.7219. Ames Nd standard was ^{143}Nd/^{144}Nd=0.511966±0.000005 (n=6) which is equivalent to ε_{Nd}=0.1. The reproducibility of this standard and the results are given as absolute values at the 2 sigma level. Total procedural blank was <10 pg for Nd.

Magnetic hysteresis loops (maximum field of 1 T) and thermomagnetic curves (applied field of 1 T from 300 to 973 K) were measured using a vibrating-sample magnetometer (VSM). Magnetic susceptibility was measured with an inductance bridge, and room-temperature remanences (e.g., anhysteretic remanent magnetization (ARM)) were measured with a 2G cryogenic magnetometer. Demagnetizations and ARM acquisition were done with a D-tech alternating field (AF) demagnetizer (maximum field of 0.2 T). Low-temperature magnetic measurements were made with a Quantum Designs superconducting susceptometer (MPMS).

4.1. Particle size

The particle size of the sediment is fairly uniform (Fig. 3), averaging to 14% sand, 74% silt, and 12% <clay, a silt loam. There is however an abrupt coarsening at 6m and another, to a lesser degree at 2.5 m. This coarsening is primarily due to an increase in sand fraction (Fig. 3). There is no consistent relationship between the percent clay and the four B_t horizons. In fact the lower two B_t horizons correspond to intervals of relative lows in clay (Fig. 3).

4.2. Mössbauer spectra

Mössbauer spectra were measured for three bulk samples. All three spectra show the same three components, a magnetic sextet, and two quadrupole doublets (Fig. 4). The sextet has a hyperfine field of around 51 T, an isomer shift of 0.37 mm, and quadrupole splitting of −0.21 mm, consistent with hematite. The sextet area ranges from 21% to 24% of the total area of the spectrum. Hematite was also found to be the

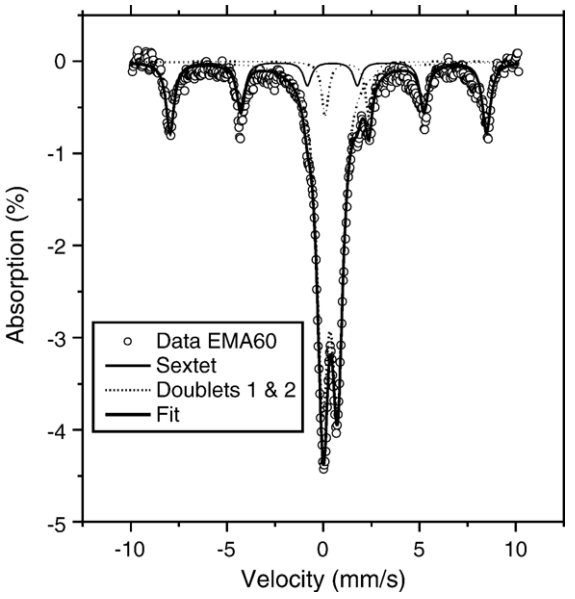

Fig. 4. Mössbauer spectrum for a bulk sample of LAA loess. All of the spectra show three components: two quadrupole doublets and a magnetic sextet. The sextet is due to hematite, and is ~20% of the total iron in the sediment.

dominant ordered magnetic mineral in samples of Pampean loess (Orgeira et al., 1998). On cooling to 77 K the hematite sextet area increases as much as 21%, indicating the presence of super-paramagnetic (SP) nano-hematite. Despite the clear magnetic sextet, the two quadrupole doublets dominate the spectrum at 300 K. The Mössbauer spectrum measured on a magnetic extract indicated that the ferrimagnetic fraction was ~50% magnetite and ~50% maghemite. It is unclear whether this result indicates two phases, a single non-stoichiometric phase which is uniformly oxidized, or some mixture of both.

4.3. Rock magnetic measurements

There is a strong covariance of ferrimagnetic susceptibility (χ_f, the total susceptibility less the high-field susceptibility determined from hysteresis loops) and anhysteretic magnetization (ARM), not shown, with saturation magnetization (J_s) (Fig. 3). (Due to the weak magnetism of hematite these parameters are primarily sensitive to the ferrimagnetic minerals in the sediment.) This covariance indicates that the major control on the variations in these parameters is the concentration of ferrimagnetic minerals. The most striking aspect of these data is the abrupt drop in susceptibility at 6 m. Though there is no consistent relationship between these simple magnetic parameters and the stratigraphy, it is worth noting that the two lowest paleosols are accompanied by obvious increases in χ_f and J_s.

4.3.1. Hysteresis loops

Hysteresis loops were unmixed using empirical basis functions (Carter-Stiglitz et al., 2001, 2002) in order to quantify the amount of nano-magnetite (<30 nm). The results were cross validated using the same technique on the low-temperature data discussed below. The ferrimagnetic fraction is dominated by SP material, ranging from ~50% to 70% (Fig. 3). We note that this technique is non-standard. However using a more common SP parameter, χ/J_s, would not change our interpretations significantly but would be less quantitative. As with χ and J_s there is no clear and consistent relationship between the SP material and the paleosols found at LAA.

4.3.2. J_s versus T (>300 K)

J_s from 273 to 973 K was measured for six samples, all of which showed similar behavior. The curves are typified by a steep linear decrease in magnetization with temperature, occurring both on cooling and warming. The curves were all non-reversible, with large increases in magnetization after heating. The increase is likely due to the conversion of some hematite to magnetite. Curie temperatures ranged from 844 to 851 K, consistent with a composition near magnetite (TM0).

4.3.3. Low-temperature magnetic data

Remanence was measured for eight samples on warming from 20 to 300 K from two initial states: zero-field cooled (ZFC) from 300 to 20 K, and field cooled (FC) in a 2.5 T field from 300 to 20 K. Fig. 5 shows typical ZFC/FC curves for the sample set. The curves are dominated by an exponential decay of remanence on warming due to the presence of SP grains, losing as much as 56% of the initial remanence. There is some elevation of FC remanences over ZFC (coming together on warming to 300 K). There is a small but noticeable change in slope near 120 K, near the Verwey transition for magnetite.

4.3.4. Partially demagnetized remanences

The magnetic identification of antiferromagnetic minerals in natural material is often quite difficult, and the quantification of their concentrations is even more so. This difficulty is due to the relative magnetic strengths of ferrimagnetic and antiferromagnetic minerals. In order to overcome this problem we have concentrated on magnetizations acquired in large fields (0.2 T<H<5 T) and then partially AF demagnetized

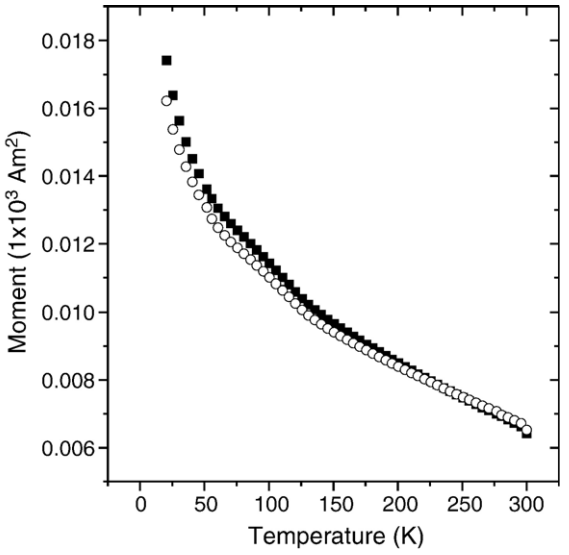

Fig. 5. Typical curves for ZFC and FC remanence on warming. The curves are nearly overlapping and show a large exponential decay in remanence on warming. Open symbols indicate ZFC, and closed indicate FC.

(maximum field of 0.2 T). This procedure offers three advantages: 1) It increases the signal-to-noise ratio (i.e. the remanence proportion of the magnetization that is due to the antiferromagnetic component is increased). 2) The treatment allows the MPMS's superconducting magnet (with fields as high as 5 T) to be used to magnetize the sample. Without the demagnetization step the unwanted magnetization produced by the magnet's residual fields (~0.05 T) produces spurious results. 3) Undemagnetized remanences acquired in fields >0.2 T were too strong to be measured on the 2G cryogenic magnetometer.

Fig. 6 shows a partial isothermal remanent magnetization (pIRM) acquisition curve for the LAA loess (actually the average of those from four samples, as the difference in the normalized curves was less than the experimental noise). The curves are close to saturation at 4 T, and there is an inflection point between 4.5 and 5 T, perhaps due to a second magnetically harder component (possibly goethite).

Fig. 7 shows room-temperature IRM's acquired in 5 T and partially AF demagnetized with 0.2 T ($^{5.0-0.2T}$IRM) measured on cooling from 300 to 20 K, warming 20–400 K, and cooling from 400 to 20 K for a sample of hematite (Nature Company, Néel temperature of 953 K—the sample used to calibrate temperature on our high-temperature VSM) (Fig. 7a), a sample of synthetic pure goethite (Guyodo et al., 2003) (Fig. 7b), and a sample of LAA loess (Fig. 7c). The goethite shows a reversible increase in $^{5.0-0.2T}$IRM on cooling between 300 and 20 K, due to an increase in spontaneous magnetization on cooling, and a completely irreversible demagnetization on warming above its Néel point. The hematite sample shows a clear Morin transition (a magnetic transition unique to hematite); as is typical for hematite the magnetization is partially reversible and hysteretic (Özdemir and Dunlop, 2002). $^{5.0-0.2T}$IRM for the LAA sample increases on cooling, and is mostly reversible. The slope decreases dramatically after heating to 400 K. Moreover, there is a large change in slope at 350 K (Fig. 7d), a Néel point consistent with aluminum-substituted or poorly crystalline goethite (Murad and Schwertmann, 1983). On heating to 400 K (a temperature above goethite's Néel temperature) and cooling back to 300 K, 7.5% of $^{5-0.2T}$IRM is lost. The Morin transition is observable (at 225 K on cooling and 250 K on warming), and shows the same hysteresis as is observed in the standard (Fig. 7b, d).

Fig. 8 shows $^{5-0.2T}$IRM on heating to 951 K in zero field. Because the sample reduces on heating (indicated by a change in color from brown-red to gray), the sample was cycled from room temperature and back to progressively higher temperatures. The curve shown in Fig. 8, after repeated heating and cooling cycles, was found to be reversible up to ~600 K. Also shown is the final cooling curve from the low-temperature experiment shown in Fig. 7d. The slopes of the two curves are remarkably continuous. There are no obvious breaks in slope in the high temperature curve, suggesting a single component. The sample's magnetization is completely unblocked at 911 K, higher than 853 K, the Curie

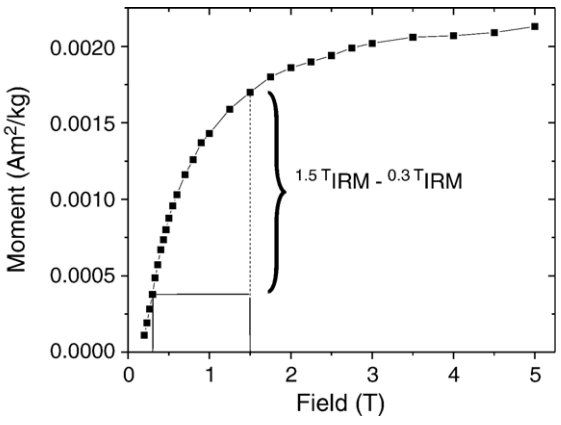

Fig. 6. The average of four normalized partial IRM acquisition curve from four separate samples. (The difference between the four curves was less than the experimental noise.) After each magnetization step the samples were partially AF demagnetized with a maximum field of 0.2 T. The highlighted magnetization indicates $^{1.5-0.3T}$IRM.

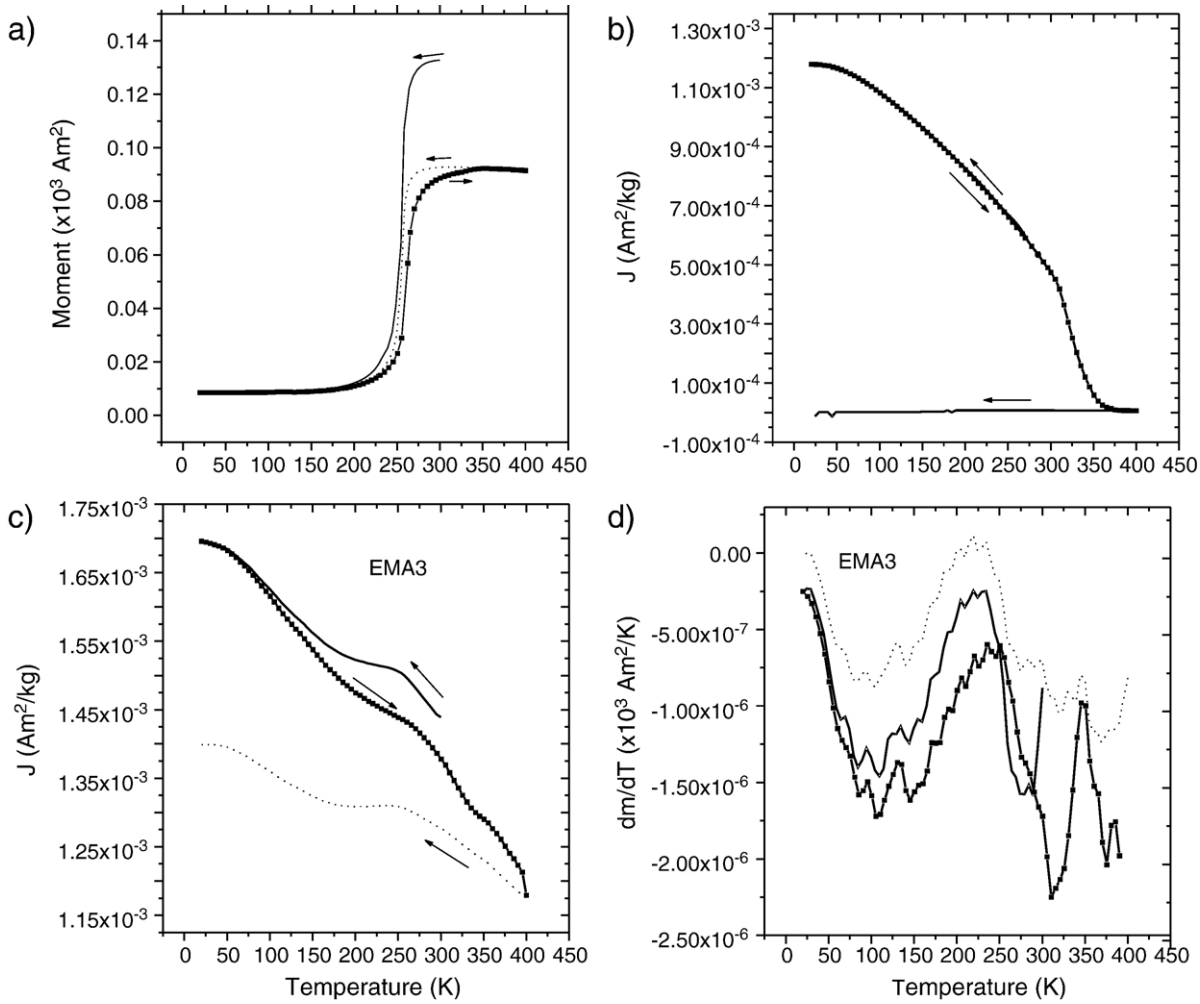

Fig. 7. Partial remanence acquired in 5 T field and then partially AF demagnetized with a maximum field of 0.2 T ($^{5.0-0.2\ T}$IRM) measured on cooling from 300–20 K, warming 20–400 K, and cooling 400–20 K for a) a hematite standard, b) a goethite standard, and c) a sample of LAA loess. d) The derivative of the curve shown in c).

temperature for magnetite, but consistent with fine-grained hematite.

In order to quantify the amount of (high coercivity) antiferromagnetic material for the entire LAA section we measured the high-coercivity component of IRM acquired in fields between 0.3 and 1.5 Tesla (T), $^{1.5-0.3T}$IRM. A DC electromagnet was used to generate the applied fields. This was done in two steps: 1) magnetizing in 0.3 T direct field, partially AF demagnetizing with 0.2 T, and measuring the remanence; 2) magnetizing in 1.5 T field partially demagnetizing as in step 1–the demagnetization typically removes ~90% of the 1.5 T remanence–and measuring the remanence. Butler (1982) used a simpler version of this technique to quantify these same minerals in red beds from New Mexico. The net result should be identical to the commonly used hard isothermal remanent magnetization (HIRM)—the extra demagnetization step was included for the reasons outlined above. This measurement was performed twice on separate sample sets and the two were averaged. Moreover, for the second sample set, $^{1.5-0.5}$IRM was also measured; while always less than $^{1.5-0.3T}$IRM the two measurements cohere exactly.

Of all of the magnetic parameters measured $^{1.5-0.3T}$IRM seems to be the most consistently related to the paleosol stratigraphy. The lowest two paleosol complexes are marked by clear highs in $^{1.5-0.3T}$IRM and so is the paleosol at 4 m (Fig. 3). Noting the incidents of incoherence, the uppermost paleosol is anticipated by an increase in $^{1.5-0.3T}$IRM and there are no low values associated with the interval of loess at 7.5 m which is

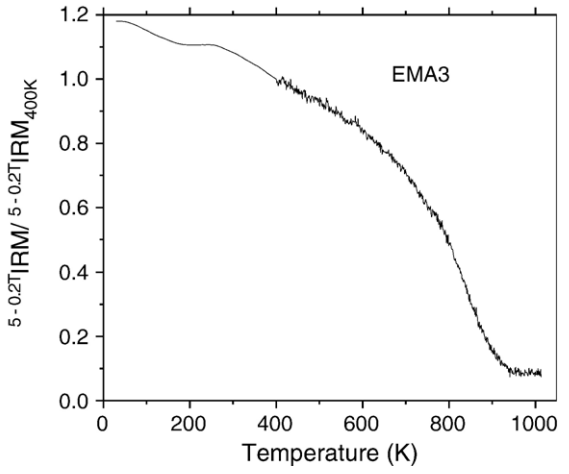

Fig. 8. $^{0.2-5T}$IRM on heating to 951 K. Also plotted is the final cooling leg (400–20 K) from Fig. 7c.

bounded by two paleosols (Fig. 3). We suspect that part of this dissonance is caused by the difficulty of visually identifying the breaks between paleosol and loess. It is also worth noting that the lowest two paleosols in the section are accompanied by peaks in both $^{1.5-0.3\ T}$IRM and both χ_f and J_s.

4.4. Major element geochemistry

Overall the major element geochemistry is fairly constant throughout the entire section. For example, the percent Si ranges from 57% to 63%, the total range only six times greater than the standard deviation. A similar homogeneity is seen for the second most abundant element in the sediment, Al (15–18%). As a point of comparison, the metamorphic and granitoid rocks suggested by Smith et al. (2003) to be the source rocks have values that range from 50% to 80% and 12% to 23% for Si and Al, respectively. The chemical index of alteration ($CIA = Al_2O/[Al_2O + CaO + Na_2O + K_2O]$) also indicates fairly homogenous sediment (Fig. 3). Not surprisingly the variation in CIA, though not much larger than 1-σ standard deviation, tracks the variation in clay fraction and SP fraction almost exactly.

4.5. Nd isotopes

ε_{Nd} at LAA ranges from −8 to −6.5, and the variation is systematic with depth. Starting with the oldest sediment, ε_{Nd} continuously becomes more negative until reaching ~−8 at around 6 m, above which it abruptly increases to ~−6.5. It then returns to −8 before increasing again to −6.5 forming a broad trough centered at ~4.5 m (Fig. 3). This broad trough is echoed in many of the other measured properties, and is seen as a broad peak in: superparamagnetic material, percent clay, and CIA (Fig. 3).

5. Discussion

5.1. Iron budget

5.1.1. "Nonmagnetic" (paramagnetic) iron-bearing minerals

The Mössbauer results demonstrate that the majority of the iron in the sediment is either paramagnetic or superparamagnetic. A large superparamagnetic contribution to the doublets is very unlikely as the spectra measured at 77 K are little changed as compared to the room temperature spectra. It is then likely that the bulk of the iron (~80%) is present in paramagnetic minerals, most likely clay minerals and biotite, which have been identified in abundance in thin section.

5.1.2. Weakly magnetic (antiferromagnetic) minerals

The second most abundant iron cache in the sediment is clearly hematite. Combining the Mössbauer results, which indicate ~20% of the total iron is bound in hematite, and the bulk geochemistry, which show typical values of ~6% (calculated as Fe_2O_3) by mass, yields ~1.5% hematite by mass. This is of the same order as the value estimated with $^{1.5-0.3T}$IRM. By assuming that the entire moment is from hematite, the hematite is SSD, grain sizes from 0.030 to 15 μm (Banerjee, 1971), and that it is saturated, one can roughly estimate the hematite concentration to be ~1%, basically in agreement with the Mössbauer data.

But is $^{1.5-0.3T}$IRM due solely to the hematite? There are two possibilities: 1) goethite is adding to the remanence, and 2) hard (relative to magnetite) maghemite is adding to remanence. On cycling from 300 → 400 → 300 K, only 7.5% of $^{5.0-0.2T}$IRM is lost. Any goethite present in the sample should be completely demagnetized (Fig. 7a). Assuming that the goethite is single domain and a reasonable M_s (~2 kA/m), this suggests non-SP goethite concentrations of only ~0.1%. Moreover, $^{1.5-0.3T}$IRM must have much less of the hard goethite moment, since the maximum field is less than 1/3 the value of that used in $^{5.0-0.2T}$IRM. Thus goethite is adding to the $^{1.5-0.3T}$IRM, but its contribution is slight and is much less than the hematite contribution. Parenthetically, this small amount of goethite does not seem sufficient to produce the observed offset in ZFC/FC curves. The offset is then likely due to SP hematite or maghemite (Kosterov, 2003). van Velzen and Zijderveld (1995) identified the presence of hard

maghemite in carbonates, such that it may not be completely demagnetized with a 0.3T AF field. Hence its possible contribution to $^{1.5-0.3T}$IRM must be addressed. The presence of such maghemite can be ruled out by the following arguments. $^{1.5-0.5T}$IRM varies in the same way as $^{1.5-0.3T}$IRM. Thus barring the existence of some extraordinarily hard maghemite, at the very least the variation in $^{1.5-0.3T}$IRM is due to changes in hematite concentration. Also, the thermal demagnetization of $^{5.0-0.2T}$IRM (Fig. 8) seems to be a single phase demagnetization. Therefore the bulk of the starting remanence must then be due to *either* hematite *or* maghemite. This then leaves no room for the 2% hematite by mass, identified by the Mössbauer and geochemistry. Therefore $^{5.0-0.2T}$IRM must be dominated by the hematite in the sample, and since $^{1.5-0.2T}$IRM is 80% of $^{5.0-0.2T}$IRM, so must $^{1.5-0.3T}$IRM.

Finally, are the variations in $^{1.5-0.3T}$IRM due to variations in hematite, or one of the other minor components, i.e., goethite? $^{1.5-0.3T}$IRM monotonically increases with the relative sextet area of the Mössbauer spectra. Moreover the range of $^{1.5-0.3T}$IRM normalized with percent iron is 10% of the maximum value; the range of the sextet area is 11% of its maximum value. The variations in $^{1.5-0.2T}$IRM are certainly due to changes in the concentration of hematite in the sediment.

5.1.3. Strongly magnetic (ferrimagnetic) minerals

Mössbauer spectroscopy (at 300 K) and X-ray diffraction measurements on magnetic extracts demonstrate that the ferrimagnetic minerals are magnetite and maghemite. The Curie temperatures confirm the Mössbauer data, implying compositions of magnetite near TM0. The concentration of the ferrimagnetic minerals can be estimated accurately using saturation magnetization, M_s (Fig. 3). The concentration of magnetite and maghemite varies between 0.1% and 0.3%. Given the high correlation of M_s with ARM and χ, the first order control on the magnetic properties of the sediment is simply the concentration of the ferrimagnetic minerals (Fig. 3).

5.2. Parent material and pedogenesis

5.2.1. Parent material

Neodymium isotopic analyses of marine sediments have been recently developed (Burton and Vance, 2000) to deduce the origin of sediments and the mechanisms responsible for particle transport (e.g., ocean circulation and aeolian transport). The same chemical analyses have been made on loess–paleosol sequences from Louchuan, China (Gallet et al., 1996). Here we follow the lead of these studies and of Smith et al. (2003) and use Nd isotopic composition of LAA loess in order to provide additional information concerning its provenance throughout the last 100 ka.

ε_{Nd} data for LAA are perfectly consistent with the Argentina-loess source model proposed by Smith et al. (2003). The range of ε_{Nd} at LAA is ~2 ε_{Nd} units; whether or not such a variation could be related to changes in grain size is not clear (Derry and France-Lanord, 1996; Goldstein et al., 1984). Consider the end-member case that the variation is controlled by changes in grain size. The changes in grain size at LAA are almost entirely due to the sand and coarse silt size fractions. Thus ε_{Nd} would be driven by changes in the parent material not pedogenesis which would be, presumably, manifested by the clay fraction.

On the other hand if ε_{Nd} is immune to fluctuations in grain size distribution and by comparing the systematic variation of ε_{Nd} at LAA to the latitudinal variation of ε_{Nd} for Andean rocks, which become more negative at lower latitudes (Futa and Stern, 1988; Hawkesworth et al., 1979), we can speculate that the exact source area for the loess is not constant with time. Instead the source is, more or less, directly to the west for the least negative values, and is to the north-west for the most negative values of ε_{Nd}. The range of ε_{Nd} could be accounted for by a north/south movement of the source of ~5°.

Assuming the wind-direction model suggested by Smith et al. (2003) the data suggest a competition between westerlies and katabatic northerlies. Between 12 and 6 m (as oxygen isotope stage 5 came to a close and glaciation increased) katabatic winds became increasingly important, followed by a sudden northward migration of the polar front causing westerlies to dominate sedimentation in the valley. The broad trough in ε_{Nd} at 4.5 m is then simply a resurgence of katabatic northerlies followed by their waning. We also point out the possibility that the variation in parent material, as indicated by ε_{Nd}, could also be driven by processes more local than large-scale changes in wind direction. For example, assuming an initial stage of fluvial transport prior to aeolian transport, changes in the fluvial system could adjust the balance of north-west and west derived sediment.

Nevertheless the ε_{Nd} indicates subtle changes in the parent material which is reflected in many of the other measured properties. Specifically, the variation in ε_{Nd} for $d<6$ m is mimicked by %-clay, CIA, and the concentration of SP material (Fig. 3). This correlation indicates that these parameters, which typically would be associated with pedogenesis, are being controlled by

the parent material. On the other hand none of the other parameters show the same slow change with depth as ε_{Nd} does for $d>6$ m (Fig. 3). For the lower half of the section we then suggest that the variation in parent material exerts little control on our suite of properties. Finally we note that $^{1.5-0.3T}$IRM varies independently of ε_{Nd} for the entire section. It is therefore unlikely that the variation in hematite concentration is controlled by variations in the parent material.

Changes in the transport processes that deliver the sediment to LAA can also affect the character of the parent material. The sand fraction of the sediment is our best tool to unravel any major changes in the transport of sediment to the site. Fortunately, it is fairly constant except at two intervals, where it increases abruptly: just above 6 and 3 m. Both of the intervals are characterized by sudden shifts to more positive values of ε_{Nd}. It is not surprising that a change in the ultimate source of the loess as indicated by ε_{Nd} is accompanied by a shift in grain size. Applying the simple logic that the distance to the source is inversely proportional to grain size, the source area seems to move farther away as it moves to the south. It is also possible, as mentioned above, that the sand fraction is controlling the changes in ε_{Nd}.

5.2.2. Pedogenesis

Unlike in China, the LAA sediment shows no consistent relationship between the enhancement of SP grains and stratigraphy. There also is no consistent magnetic depletion of the sediment with pedogenesis as observed in Alaska (Begét, 2001; Vlag et al., 1999) and suggested for Las Carreras (Schellenberger et al., 2003). Furthermore the correlations between ε_{Nd} and SP material, CIA, and clay demonstrate that these common indicators of pedogenesis are at least in part controlled by changes in the parent material. Neither CIA nor the clay fraction shows a consistent relationship with the identified B_t horizons, where clay illuviation is clearly the present. In fact, two of the B_t horizons correspond to relative lows in clay fraction. This again implies that at least some of the variation in clay fraction is due to changes in the parent material, and not clay illuviation. What are powerful pedogenic indicators in China are, at LAA, a palimpsest of allochthonous and in situ pedogenic forcings.

Hematite is a common product of pedogenesis, and there is then some reason to suspect, a priori, that the hematite in our section is a pedogenic product. There are several pieces of circumstantial evidence that suggest that the variations in hematite are due to variations in the degree of pedogenesis: 1) The climatic regime, i.e. yearly precipitation and average temperature, is such that one would expect hematite formation (Schwertmann, 1988). 2) The Eh (inferred from the absence of preserved carbon) and pH (Zinck and Syago, 2001) of loess–paleosols are such that hematite is predicted to be a pedogenic product (Retallack, 2001). Furthermore the copious amounts of iron (>5%) in the sediment provide ample raw material for hematite formation. 3) The data suggest that much of the hematite is fined-grained: SP hematite has been identified in the Mössbauer spectra, the absence of strong Morin transition, and abundant translucent hematite has been identified in thin Section. 4) The paleosol stratigraphy shows a reasonable, albeit far from perfect, correlation with the hematite concentration. 5) Hematite forming in situ has been identified in thin section, and with electron microscopy. Fig. 9a shows red (both in plane-polarized, & cross-polarized light) amorphous material which is opaque in its thickest portion, filling the space between allochthonous grains. The material is interpreted to be hematite forming in situ. The abundant biotite in the loess provides two chemical pathways to hematite: 1) the transformation of biotite to clay can produce hematite, 2) ferrous iron can be leached from biotite which often leads to the precipitation of hematite on its edges (Murakami et al., 2003). Biotite weathering is also relatively rapid, up to ~10 times more rapid than the weathering of feldspars (Blum and Erel, 1997). Fig. 9b, and c show Fe and Ti elemental maps for a biotite grain. The titanium-free iron lath is red in transmitted light (plane polarized and cross-polarized), and is interpreted as hematite. The fact that it is titanium free is consistent with it being a weathering product, and its morphology and location with respect to the biotite grain suggest that it has formed in situ. There is also noticeable iron zoning in the biotite grain, with the edges having less iron as it is being progressively leached from the outside. Fig. 9d shows an iron map for a nodule-like aggregate. The outer outlined region indicates an area that is red in transmitted light (plane-polarized and cross-polarized). The inner outlined regions indicate a region with high titanium and iron. The highlighted iron "rings" are clearly grain coatings, and are titanium free. The interpretation is that the iron–titanium grain is detrital and weathering to form the hematite nodule, and coatings on nearby grains. Although there is ample evidence for hematite forming in situ, not all of the translucent hematite is as convincingly formed in situ. For example, the morphology of the grain shown in Fig. 9e is difficult to interpret. The fact that the lowest value of $^{1.5-0.3T}$IRM is still ~70% of the maximum value

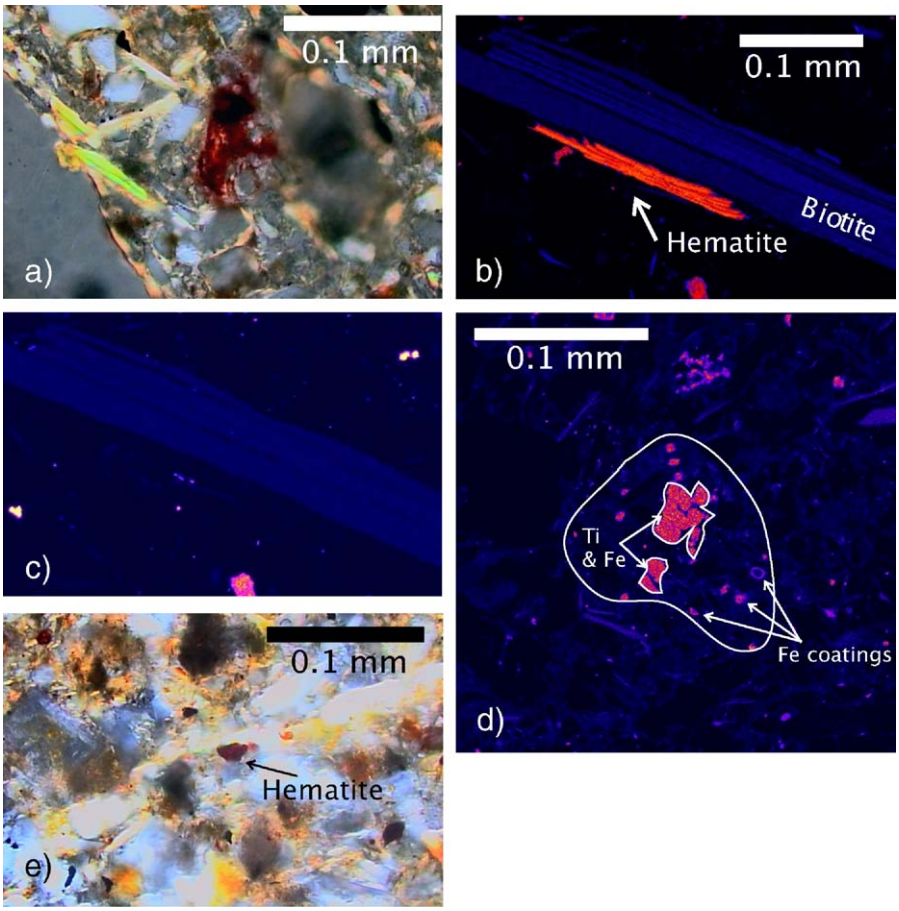

Fig. 9. All microscope images are in cross-polarized light. a) Red amorphous material which is opaque in its thickest portion, most likely hematite, filling the space between allochthonous grains. Element maps of biotite grain with associated hematite of b) Fe and c) Ti. d) Fe element map of nodule-like aggregate. e) Hematite of unknown genesis. (For interpretation of the references to colour in this figure legend, the reader is referred to the web version of this article.)

suggests a baseline amount of hematite being brought in as detritus. The overall uniformity of the major element geochemistry, and the identified presence of in situ pedogenic hematite suggests, however, that the *variations* in $^{1.5-0.3T}$IRM are due to changes in the in situ pedogenic hematite.

The lowest two paleosols not only show peaks in hematite concentration but also the concentration of ferromagnetic minerals. Surprisingly obvious peaks are not observed in the SP fraction, CIA, or clay fraction. Perhaps these two lowest paleosols, both in oxygen isotope stage 5, represent time intervals when the pedogenic regime has moved toward that seen in China, where the pedogenic formation of ferromagnetic minerals is important. The subtler grain-size dependence of these pedogenic ferromagnetic grains could be masked by changes in parent material, which are obviously controlling factors higher in the section.

5.3. Chronology

The OSL age estimates suggest sedimentation rates a factor of five larger than those estimated for La Mesada (Kemp et al., 2003) and Las Carreras (Schellenberger et al., 2003). One possible explanation for this discrepancy is, of course, error in the age estimates presented in this study. A careful examination of the fidelity of the LAA ages will not only address the contrasting sedimentation rates, but also the overall quality of the LAA chronology.

An overestimation of the dose exposure of the LAA samples is not likely as they are younger than the OSL ages from La Mesada, and would correspond to the uppermost, youngest portion of the Las Carreras section. An underestimation of dose exposure cannot be ruled out so easily. One possible source of an underestimation is post-sampling exposure to light. While this cannot be

ruled out completely, it is unlikely as the plastic sampling tubes were covered in multiple layers of opaque tape. Anomalous fading could also lead to an underestimation of the dose exposure. This possibility seems unlikely as quartz is thought to not suffer from anomalous fading (Wantanuki and Tsukmoto, 2001). An overestimation of the dose rate could also be a source of error in the age estimates, giving younger than actual ages. Average water contents higher than the modern values would lead to this overestimation. However, the difference between wet and dry dose rates for the LAA samples is only ~20%, and thus not likely to be a large source of error in the dating. Although there is no specific reason to discard the LAA OSL dates, their fidelity would be improved greatly on reproduction, by means of OSL or otherwise.

The abrupt change in the sediment at 6 m (Fig. 3), in some sense, corroborates the chronology. According to the chronology this change in texture occurred at ~72 kya. Within the error of the chronology, this corresponds to the beginning of oxygen-isotope stage 4. In other words, the chronology predicts that 6 m is where we would expect the most radical change in climate and paleoenvironment, glacial to interglacial. It is exactly at this level that we find remarkable changes in the empirical data, indicating simultaneous changes, be them ephemeral or permanent, in source, transport, and degree of alteration.

The different topographic setting of the LAA section compared to La Mesada and Las Carreras can explain the difference in sedimentation rate between our site and the two from the valley center.

The chronology is, of course, a crucial factor in determining how continuous sediment deposition at LAA was. In order to answer this question in a satisfying manner much more detailed dating must be accomplished.

5.4. Climate paleorecord?

On comparing our record to the coeval paleoclimate record from Antarctica (Vostok) (Sowers et al., 1993), we see some similarity, e.g., all of the troughs in the LAA section correlate with troughs in the Vostok record (Fig. 10). To assess the degree of correlation we use singular spectrum analysis (SSA) to filter the time series and directly compare the two different climate proxies (Vautard et al., 1992). The two time series were linearly interpolated with a time interval of 0.3 ky for the period 100–59 kya, and all but the first three terms of the SSA transform were filtered. The filtered time series correlate with the original time series with $R > 0.91$. The chronology of the LAA time series was adjusted slightly using the solid tie lines shown in Fig. 10; the adjusted chronology is well within the error of the original chronology. The coherence was calculated between the

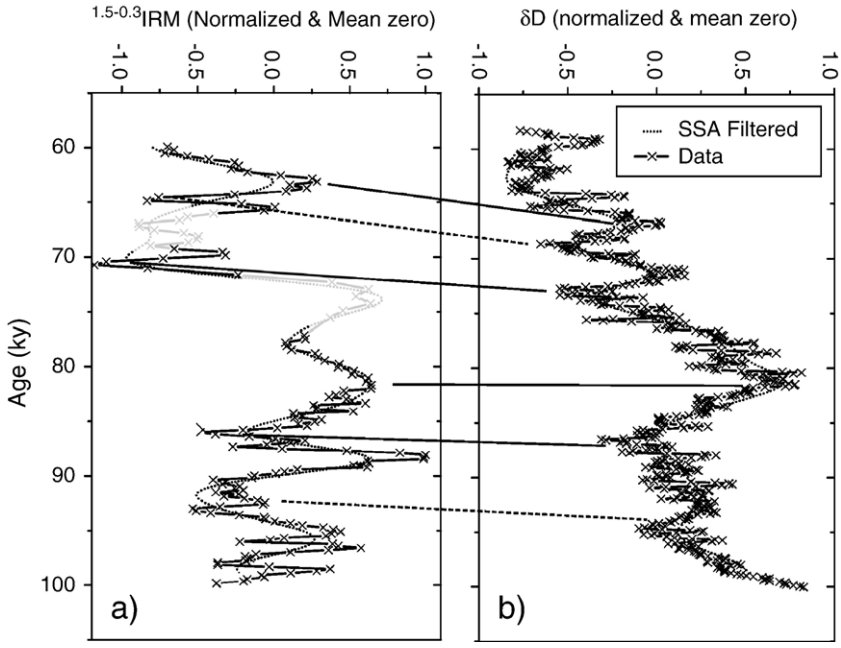

Fig. 10. a) The LAA hematite proxy (3-point running average), (b) Vostok δD time series and their filtered counterparts using the first three terms of a SSA transform. The grey LAA data indicate field-identified intervals of resedimentation.

two time series giving an $R=0.71$. Since we have included the whole of the LAA section, including the resedimented portions, the coherence value is a lower bound. The two records clearly vary in similar ways.

A similar quality of correlation is observed between the hematite concentration at LAA and speleothem oxygen isotope data from Southern Brazil (Cruz et al., 2005), i.e., peaks and troughs are easily matched. For example both records have prominent peaks at ~80 kya. Notable differences are however apparent; the strong precessional cycle observed by Cruz et al. (2005) is not apparent at LAA. The strong peak in hematite at ~88 kya at LAA corresponds to a small peak in a deep precessional trough in the speleothem record. If these differences truly reflect contrasting paleoclimates at the two sites, rather than an imperfect paleoclimate recording, it has consequences concerning the climate dynamics of the continent. Such differences are not unexpected considering that LAA is situated at the limit of the monsoonal circulation and the strong orographic controls on precipitation at the site.

Assuming the changes in hematite at LAA are driven by changes in pedogenesis, there are three plausible driving forces: changes in sedimentation rate, changes in temperature, and changes in soil humidity (presumably driven by changes in local precipitation). As argued above, changes in sedimentation rate are not likely to be drastic enough to, alone, cause major changes in pedogenesis. The changes in late Pleistocene paleotemperature at the site were probably not more than a few °C, not enough to significantly change the kinetics of the weathering reactions, and thus would not have changed the production rates of hematite. The supply of moisture to the site is then the most likely control on the weathering rates at LAA.

Sea surface temperatures (SST) of the South Atlantic are likely to control the strength of the SASM. As the SST increases, the moisture available to the low level SASM flow increases, and precipitation delivered to the LAA site increases. The Vostok record gives some sense of the variation in South Atlantic SST, and the coherence of the two time series then suggests that the major control on precipitation at LAA is the SST of the South Atlantic. Another important control on modern precipitation at LAA is the degree of southward displacement of the intertropical convergence zone (ITCZ) during the austral summer (Chang et al., 1997; Trauth et al., 2000). Reducing the extent of this southern migration would also result in a reduction of precipitation at LAA.

How reliable is the above correlation? The answer lies in our understanding of the processes that control the hematite concentration in the sediment, and the history of sedimentation. Although at this stage there are too many outstanding or poorly constrained questions to address this question completely, the similarity of the two records seems too great to dismiss. Clearly, a detailed chronology demonstrating the history of sedimentation, and a more complete understanding of the variations in hematite are the two primary areas which need to be addressed.

6. Conclusions

The OSL chronology indicates that the maximum age for the cessation of loess deposition for the valley is ~60 kya. Although the LAA section roughly correlates to the upper portion of the La Carreras section, our chronology indicates much higher sedimentation rates at LAA. This is probably due to the different topographic settings of the sections, i.e., LAA proximity to the valley wall.

Unlike the Chinese or Alaskan loess, no consistent relationship between the stratigraphy and the ferrimagnetic minerals in the sediment is observed. Through a combination of geochemistry, Mössbauer, X-ray diffraction, and rock magnetic measurements an iron budget was calculated for the LAA loess, indicating that 80% of the iron is in paramagnetic material (likely biotite, and clay minerals), 20% hematite, and less than a percent in goethite and ferrimagnetic magnetite/maghemite. Moreover, changes in the paramagnetic, hematite, and ferrimagnetic components have been quantified for the entire section using rock magnetic measurements. We hope that this quantification, especially of the finest-grained and highest-coercivity weakly magnetic hematite in the presence of a dominant ferrimagnetic background, will be an approach that will lead to a better understanding of the iron in this and other loess–paleosol sequences. This remains an important problem, especially in light of the fact that an understanding of the most abundant iron oxide, i.e. hematite, in the most studied loess deposits in the world, i.e. the Chinese loess, has not yet emerged.

Our initial interpretation of the variations in hematite is that they are driven by changes in the degree of in situ pedogenesis. The variation of hematite concentration is further interpreted as being sensitive to the amount of available moisture at the site, increasing above its base value as moisture increases. Thus the observed correlation of the LAA hematite record with the Vostok hydrogen isotope record is explained by changes in the strength of the South American Summer Monsoon.

In order to test the fidelity of the LAA record several questions should be further explored: 1) A more detailed chronology for the LAA section must be established to test the initial chronology presented in this study, and to provide a detailed history of sedimentation. 2) A more complete understanding of the processes governing the variation in hematite is needed. 3) It is necessary to reproduce the record elsewhere in Tafi del Valle, or at another nearby location. Moreover a valley-wide loess stratigraphy needs to be established. 4) A complete micromorphological study at LAA would add immensely to our knowledge of pedogenesis at the site.

The Tafi loess spans an enormous age interval and thus there is a potential for longer paleoclimate records from the area. Moreover, the loess is not likely to be limited to Tafi del Valle, and undiscovered loess deposits most likely exist in the immediate area in similar inter-montane valleys. Given the lack of paleorecords from this region, and the uncertainty concerning climate dynamics–e.g., the exact nature of interhemispheric climate links (Markgraf and Seltzer, 2001)–the records of abrupt climate change archived in the loess of northern Argentina are certain to become important.

Acknowledgements

This is IRM contribution number 0602. IRM is supported by the Instrumentation and Facilities Program, Earth Science Division, National Science Foundation. Electron microprobe analyses were carried out at the Electron Microprobe Laboratory, Department of Geology and Geophysics, University of Minnesota-Twin Cities. Thanks to Fawna Korhonen for her invaluable help with the electron microscopy work. Finally, thanks to M.J. Orgeira for all of her help concerning this study.

References

Adamiec, G., Aitken, M., 1998. Dose–rate conversion factors: update. Ancient TL 16 (2), 37–50.

Banerjee, S.K., 1971. New grain-size limits for paleomagnetic stability in hematite. Nature. Physical Science 232, 15–16.

Banerjee, S.K., Hunt, C.P., Liu, X.-M., 1993. Separation of local signals from the regional paleomonsoon record of the Chinese loess plateau: a rock-magnetic approach. Geophysical Research Letters 20, 843–846.

Begét, J.E., 2001. Continuous Late Quaternary proxy climate records from loess in Beringia. Quaternary Science Reviews 20, 499–507.

Begét, J.E., Stone, D.B., Hawkins, D.B., 1990. Paleoclimatic forcing of magnetic susceptibility variations in Alaskan loess during the Late Quaternary. Geology 18, 40–43.

Blasi, A., Zárate, M., Kemp, R., 2001. Sedimentación y pedogénesis cuaternaria en el noreste de la pampa bonaerense: la localidad gorina como caso de estudio. Revista Argentina de Sedimentología 8 (1), 77–92.

Blott, S.J., Pye, K., 2001. Gradistat: a grain size distribution and statistics package for the analysis of unconsolidated sediments. Earth Surface Processes and Landforms 26, 1237–1248.

Blum, J., Erel, Y., 1997. Rb–Sr isotope systematics of a granitic soil chronosequence; the importance of biotite weathering. Geochimica et Cosmochimica Acta 61 (15), 3193–3204.

Burton, K.W., Vance, D., 2000. Glacial–interglacial variations in the neodymium isotope composition of seawater in the Bay of Bengal recorded by planktonic foraminifera. Earth and Planetary Science Letters 176 (3–4), 425–441.

Butler, R.F., 1982. Magnetic mineralogy of continental deposits, San Juan Basin, New Mexico, and Clark's Fork Basin, Wyoming. Journal of Geophysical Research B: Solid Earth 87, 7843–7852.

Carter-Stiglitz, B.S., Moskowitz, B.M., Jackson, M.J., 2001. Unmixing magnetic assemblages, and the magnetic behavior of bimodal mixtures. Journal of Geophysical Research B: Solid Earth 106 (B11), 26, 397–26, 411.

Carter-Stiglitz, B., Banerjee, S.K., Solheid, P.A., Jackson, M., Moskowitz, B., 2002. Unmixing Argentine Loess, 20th Course of the International School of Geophysics: Fundamental Rock Magnetism and Environmental Applications. "Ettore Majorana" Foundation and Centre for Scientific Culture, Erice, Italy, pp. 19–21.

Chang, P., Ji, L., Li, H., 1997. A decadal climate variation in the tropical Atlantic Ocean from thermodynamic air–sea interactions. Nature 385, 516–518.

Chlachula, J., Evans, M.E., Rutter, N.W., 1998. A magnetic investigation of a Late Quaternary loess/palaeosol record in Siberia. Geophysical Journal International 132 (1), 128–132.

Cruz, F.W., et al., 2005. Insolation-driven changes in atmospheric circulation over the past 116,000 years in subtropical Brazil. Nature 434, 63–66.

Dearing, J.A., Hannam, J.A., Anderson, A.S., Wellington, E.M.H., 2001. Magnetic, geochemical and DNA properties of highly magnetic soils in England. Geophysical Journal International 144 (1), 183–196.

Derry, L.A., France-Lanord, C., 1996. Neogene Himalayan weathering history and river $^{87}Sr/^{86}Sr$: impact on the marine Sr record. Earth and Planetary Science Letters 142, 59–74.

Evans, M.E., Heller, F., 2001. Magnetism of loess/paleosol sequences: recent developments. Earth-Science Reviews 54, 129–144.

Evans, M.E., Heller, F., 2003. Environmental Magnetism: Principles and Applications of Environmagnetics. Academic Press, Elsevier Science, Amsterdam.

Evans, M.E., Rokosh, C.D., 2000. The last interglacial in the Chinese loess plateau: a petromagnetic investigation of samples from a north–south transect. Quaternary International 68–71, 77–82.

Eyre, J.K., Dickson, D.P.E., 1995. Mössbauer spectroscopy analysis of iron-bearing minerals in the Chinese loess. Journal of Geophysical Research B: Solid Earth 100, 17,925–17, 930.

Fine, P., Verosub, K.L., Singer, M.J., 1995. Pedogenic and lithogenic contributions to the magnetic susceptibility record of the Chinese loess/palaeosol sequence. Geophysical Journal International 122, 97–107.

Forman, S.L., 1991. Late Pleistocene chronology of loess deposition near Luochuan, China. Quaternary Research 36 (1), 19–28.

Futa, K., Stern, C., 1988. Sr and Nd isotopic and trace element composition of Quaternary volcanic centres of the southern Andes. Earth and Planetary Science Letters 88, 253–262.

Gallet, S., Jahn, B., Torii, M., 1996. Geochemical characterization of the Luochuan loess–paleosol sequence, China, and paleoclimatic implications. Chemical Geology 133, 67–88.

Goldstein, S.L., O'Nions, P.J., Hamilton, P.J., 1984. A Sm–Nd isotopic study of atmospheric dust particulates from major river systems. Earth and Planetary Science Letters 70, 221–236.

Guyodo, Y., Mostrom, A., Penn, R.L., Banerjee, S.K., 2003. From Nanodots to Nanorods: oriented aggregation and magnetic evolution of nanocrystalline goethite. Geophysical Research Letters 30 (10), 22.

Hawkesworth, C., et al., 1979. $^{143}Nd/^{144}Nd$, $^{87}Sr/^{86}Sr$ and incompatible element variations in chalk–alkaline andesites and plateau lavas from South America. Earth and Planetary Science Letters 42, 45–57.

Heller, F., Evans, M.E., 1995. Loess magnetism. Reviews of Geophysics 33, 211–240.

Heller, F., Liu, T.-S., 1982. Magnetostratigraphical dating of loess deposits in China. Nature 300, 431–433.

Heller, F., Liu, T.-S., 1984. Magnetism of Chinese loess deposits. Geophysical Journal of the Royal Astronomical Society 77, 125–141.

Heller, F., Liu, T.-S., 1986. Palaeoclimatic and sedimentary history from magnetic susceptibility of loess in China. Geophysical Research Letters 13, 1169–1172.

Hunt, C.P., et al., 1995a. Rock-magnetic proxies of climate change in the loess–paleosol sequences of the western loess plateau of China. Geophysical Journal International 123, 232–244.

Hunt, C.P., Moskowitz, B.M., Banerjee, S.K., 1995b. Magnetic properties of rocks and minerals. In: Ahrens, T.J. (Ed.), A Handbook of Physical Constants, vol. 3. American Geophysical Union, Washington, DC, pp. 189–204.

Iriondo, M., 1990. Map of the South American plains—its present state. Quaternary of South America and Antarctic Peninsula, vol. 6. Balkema, Amsterdam, pp. 297–308.

Iriondo, M.H., 1997. Models of deposition of loess and loessoids in the Upper Quaternary of South America. 10, 71–79.

Iriondo, M.H., 1999. Climatic changes in the South American plains: records of a continent-scale oscillation. Quaternary International 57–58, 93–112.

Iriondo, M., 2002. Comment on "Genesis and distribution of the late Pleistocene and Holocene loess of Argentina: a regional approximation", by J. Sayago, M. Collantes, A. Karlson, and J. Sanabria. Quaternary International 95–96, 209–210.

Ji, J., Balsam, W., Chen, J., 2001. Mineralogic and climatic interpretations of the Luochuan loess section (China) based on diffuse reflectance spectrophotometry. Quaternary Research 56 (1), 23–30.

Kemp, R., et al., 2003. Micromorphology and OSL dating of the basal part of the loess–paleosol sequence at La Mesada in Tucumán province, northwest Argentina. Quaternary International 106–107, 111–117.

Kemp, R., Toms, P., King, M., Kröhling, D., 2004. The pedosedimentary evolution and chronology of Tortugas, a Late Quaternary type-site of the northern Pampa, Argentina. Quaternary International 114 (1), 101–112.

Kosterov, A., 2003. Low-temperature magnetization and AC susceptibility of magnetite: effect of thermomagnetic history. Geophysical Journal International 154 (1), 58–71.

Krohling, D.M., 1999. Sedimentological maps of the typical loessic units in North Pampa, Argentina. Quaternary International 62, 49–55.

Kukla, G.J., An, Z.-S., 1989. Loess stratigraphy in central China. Palaeogeography, Palaeoclimatology, Palaeoecology 72, 203–225.

Kukla, G., et al., 1988. Pleistocene climates in China dated by magnetic susceptibility. Geology 16, 811–814.

Liu, X.-M., Liu, T.-S., Cheng, M.Y., Liu, C., Xu, T.-C., 1985. The primary study on magnetostratigraphy of a loess profile in Xifeng area, Gansu Province. International Symposium on Loess Research, Xian, China, p. 5.

Liu, X.M., Hesse, P., Rolph, T., Beget, J.E., 1999. Properties of magnetic mineralogy of Alaska loess: evidence for pedogenesis. Quaternary International 62, 93–102.

Lu, Y., Prescott, R., Robertson, B., Hutton, J.D., 1987. Thermoluminescence dating of the Malan loess at Zhaitang. Geology 15 (7), 603–605.

Maher, B.A., 1998. Magnetic properties of modern soils and Quaternary loessic paleosols; paleoclimatic implications. Palaeogeography, Palaeoclimatology, Palaeoecology 137 (1–2), 25–54.

Maher, B.A., Thompson, R., 1991. Mineral magnetic record of the Chinese loess and paleosols. Geology 19, 3–6.

Markgraf, V., Seltzer, G. (Eds.), 2001. Pole–Equator–Pole Paleoclimates of the Americas Integration: Toward the Big Picture. Interhemispheric Climate Linkages. Academic Press, London.

Matasova, G., Petrovsky, E., Jordanova, N., Zykina, V., Kapicka, A., 2001. Magnetic study of Late Pleistocene loess/palaeosol sections from Siberia: palaeoenvironmental implications. Geophysical Journal International 147 (2), 367–380.

Morrás, H., 1999. Geochemical differentiation of Quaternary sediments from the Pampean region based on soil phosphorus contents as detected in the early 20th century. Quaternary International 62, 56–57.

Murad, E., Schwertmann, U., 1983. The influence of aluminium substitution and crystallinity on the Mossbauer spectra of goethite. Clay Minerals 18 (3), 301–312.

Murakami, T., Ustunomiya, S., Yokoyama, T., Kasama, T., 2003. Biotite dissolution processes and mechanisms in the laboratory and in nature; early stage weathering environment and vermiculitization. American Mineralogist 88 (2–3).

Murray, A.S., Wintle, A.G., 2000. Luminescence dating of quartz using an improved single-aliquot regenerative-dose protocol. Radiation Measurements 32, 57–73.

Orgeira, M.J., Walther, A.M., Vásquez, C.A., Di Tommaso, I., Alonso, S., Sherwood, G., Yuguan, Hu, Vilas, J.F.A., 1998. Mineral magnetic record of paleoclimate variation in loess and paleosol from the Buenos Aires formation (Buenos Aires, Argentina). Journal of South American Earth Sciences 11 (6), 561–570.

Özdemir, O, Dunlop, D.J., 2002. Thermoremanence and stable memory of single-domain hematites. Geophysical Research Letters 29 (18).

Retallack, G., 2001. Soils of the Past: an Introduction to Paleopedology. Blackwell Science, Malden, MA.

Sayago, J.M., 1995. The Argentine neotropical loess: an overview. Quaternary Science Review 14, 755–766.

Sayago, J.M., Collantes, M.M., Karlson, A., Sanabria, J., 2001. Genesis and distribution of the Late Pleistocene and Holocene loess of Argentina: a regional approximation. Quaternary International 76/77, 247–257.

Schellenberger, A., Heller, F., Veit, H., 2003. Magnetostratigraphy and magnetic susceptibility of the Las Carreras loess–paleosol

sequence in Valle de Tafí, Tucumán, NW-Argentina. Quaternary International 106–107, 159–167.

Schwertmann, U., 1988. Occurrence and formation of iron oxides in various pedoenvironments. In: Stucki, J.W., Goodman, B.A., Schwertmann, U. (Eds.), Iron in Soils and Clay Minerals. Reidel Publishing, Dordrecht, pp. 267–308.

Smith, J., et al., 2003. Isotopic constraints on the source of Argentinian loess—with implications for atmospheric circulation and the provenance of Antarctic dust during recent glacial maxima. Earth and Planetary Science Letters 212 (1–2), 181–196.

Sowers, T.M., et al., 1993. 135 000 year Vostok—SPECMAP common temporal framework. Paleoceanography 8, 737–766.

Terrugi, M.E., 1957. The nature and origin of Argentine loess. Sedimentary Petrology 27 (3), 322–332.

Tonni, E.P., et al., 1999. The Ensenada and Buenos Aires formations (Pleistocene) in a quarry near La Plata, Argentina. Journal of South American Earth Sciences 12 (3), 273–291.

Trauth, M.H., Hermanns, R.L., Strecker, M.R., Alonso, R., Haselton, K., 2000. Climate change and mass movements in the NW Argentine Andes. Earth and Planetary Science Letters 179 (2).

van Velzen, A.J., Zijderveld, J.D.A., 1995. Effects of weathering on single-domain magnetite in Early Pliocene marine marls. Geophysical Journal International 121, 267–278.

Vautard, R., Yiou, P., Ghil, M., 1992. Singular-spectrum analysis: a toolkit for short, noisy chaotic signals. Physica D 95–126.

Verosub, K.L., Fine, P., Singer, M.J., TenPas, J., 1993. Pedogenesis and paleoclimate: interpretation of the magnetic susceptibility record of Chinese loess–paleosol sequences. Geology 21, 1011–1014.

Vlag, P.A., Oches, E.A., Banerjee, S.K., Solheid, P.A., 1999. The paleoenvironmental–magnetic record of the Gold Hill Steps loess section in central Alaska. Physics and Chemistry of the Earth 24 (9), 779–783.

Wantanuki, T., Tsukmoto, S., 2001. A comparison of GLSL, IRSL, and TL dating methods using loess deposits from Japan and China. Quaternary Science Reviews 20, 847–851.

Zárate, M., 2003. Loess of South America. Quaternary Science Reviews 22 (18–19), 1987–2006.

Zárate, M., Kemp, R., Blasi, A., 2002. Identification and differentiation of Pleistocene paleosols in the northern Pampas of Buenos Aires, Argentina. Journal of South American Earth Sciences 15, 303–313.

Zhou, J., Lau, K.M., 1998. Does a monsoon climate exist over South America? Journal of Climate 11 (5), 1020–1040.

Zhou, L.-P., Oldfield, F., Wintle, A.G., Robinson, S.G., Wang, J.T., 1990. Partly pedogenic origin of magnetic variations in Chinese loess. Nature 346, 737–739.

Zinck, J.A., Syago, J.M., 2001. Climatic periodicity during the Late Pleistocene from loess–paleosol sequence in northwest Argentina. Quaternary International 78, 11–16.